Remote Sounding of the Tropical Cirrus Cloud Temperature and Optical Depth Using 6.5 and 10.5 μm Radiometers during STEP

K. N. LIOU, S. C. OU AND Y. TAKANO

Department of Meteorology/CARSS, University of Utah, Salt Lake City, Utah

F. P. J. VALERO

Space Science Division, NASA Ames Research Center, Moffett Field, California

T. P. ACKERMAN

Department of Meteorology, Pennsylvania State University, University Park, Pennsylvania

ABSTRACT

A dual-channel retrieval technique involving the water vapor band at 6.5 μm and the window region at 10.5 μm has been developed to infer the temperature and emissivity of tropical anvils. This technique has been applied to data obtained from the ER-2 narrow field-of-view radiometers during two flights in the field observation of the Stratosphere-Troposphere Exchange Project (STEP) near Darwin, Australia, January–February 1987. The retrieved cloud temperatures are between 190 and 240 K, while the cloud emissivities derived from the retrieval algorithm range from about 0.2 to 1. Moreover, the visible optical depths have been obtained from the cloud emissivity through a theoretical parameterization with values of 0.5–10. A significant portion of tropical cirrus clouds are found to have optical depths greater than about 6. Because of the parameterization, the present technique is unable to precisely determine the optical depth values for optically thick cirrus clouds.

1. Introduction

Cirrus clouds are largely composed of nonspherical ice crystals and are generally semitransparent and nonblack due to the low concentration of ice crystals. Because of high locations and low temperatures, they trap a significant amount of thermal infrared radiation emitted from the warmer surface and low atmosphere. The importance of cirrus clouds in climate has been discussed extensively by Liou (1986). Accurate mapping of their geometrical and optical properties from space, on a global scale, is critically significant to understanding the role of cirrus in climate and climatic perturbations due to various radiative forcings, such as the anticipated increase in carbon dioxide.

Numerous methodologies have been proposed to infer cirrus information using satellite infrared channels. Liou (1977) presented a method using four wavelengths in the 10 μm window region to determine the cloud thickness and emissivity. Szejwach (1982) developed a technique based on the channels in the water vapor vibrational–rotational band and the 10 μm window region to derive the cirrus temperature and emissivity using METEOSAT data. In a similar approach, Pollinger and Wendling (1984) used the 6.3 and 11.0

μm wavelengths to infer the height of optically thin ice clouds. Huang and Liou (1984) described a dual channel and dual scanning angle technique for determining the cirrus optical depth and temperature, which uses the 3.7 and 10.8 μm channels from the Advanced Very High Resolution Radiometer (AVHRR).

In this paper we develop a retrieval method for the determination of the optical depth and temperature of tropical anvils from data measured by the NASA ER-2 6.5 and 10.5 μm downward viewing, narrow field-of-view radiometers. These data were obtained during the Stratosphere–Troposphere Exchange Project (STEP), which was carried out in the vicinity of Darwin, Australia in early 1987. One of the objectives of the STEP was to investigate the mechanisms controlling the formation and dissipation of cirrus anvils in connection with the observed extreme dryness of the stratosphere. The instruments on the NASA ER-2 aircraft included dual-channel, narrow field-of-view radiometers at 6.5 and 10.5 μm, and hemispheric broadband infrared and solar radiometers. During the latter part of January and the first part of February 1987, a total of 14 missions were flown. In reviewing the available data and satellite cloud pictures, we find that there were well-defined clear and cirrus overcast regions during the ninth and twelfth flights. For this reason, we have selected the radiation data associated with these flights for the retrieval analysis. In section 2 of this

---

Corresponding author address: Professor Kuo-Nan Liou, Dept. of Meteorology/CARSS, University of Utah, Salt Lake City, UT 84112.

paper, we present a dual-channel algorithm for the retrieval of the cirrus temperature and emissivity, including a discussion on the parameterization of the emissivity of cirrus clouds in terms of the 0.55 μm visible optical depth. Section 3 describes the application of the retrieval algorithm to the STEP data. Finally, conclusions are given in section 4.

2. Determination of cirrus emissivity and temperature from 6.5 and 10.5 μm channels

In order to develop a retrieval method for the inference of the cirrus temperature and emissivity based on two radiance observations, a number of parameterizations and simplifications for atmospheric and cloud variables are necessary. Among these variables we must examine the behavior of the cloud emissivity in terms of its dependence on wavelength and cloud parameters.

The monochromatic upwelling cloud emissivity, simply referred to as the cloud emissivity, for applications to satellite remote sensing, is defined by

$$\epsilon_\nu = I_\nu^\uparrow (z_t)/B_\nu(T_c), \qquad (1)$$

where z_t denotes the cloud top height, T_c the cloud temperature, B_ν the Planck function for a given wavenumber, ν, and $I_\nu^\uparrow$ the upwelling radiance at the cloud top when the upward and downward radiances at the cloud base and top, respectively, are set to zero. By virtue of the definition of the cloud emissivity, it is independent of the atmospheric temperature and humidity profiles and cloud position. However, it is a function of numerous parameters, including wavenumber, cloud temperature, cloud thickness, and ice crystal size distribution.

We first examine the dependence of the cloud emissivity on the cloud temperature in the case of high tropical cirrus clouds. A cirrostratus (Cs) ice crystal size distribution (Heymsfield 1975) was used in light scattering and radiative transfer calculations (Takano and Liou 1989a,b). The averaged cloud temperatures were varied from 200 to 220 K. The computed cloud emissivities for these two temperatures using cloud thicknesses of 0.1, 0.5, 1, and 2 km differ only in the fifth decimal point. It follows that the dependence of the cloud emissivity on cloud temperature is insignificant. This is because the upwelling radiance at the cloud top and Planck function are both functions of temperature and the ratio operation largely removes this functional dependence. This conclusion is valid for 10.5 as well as 6.5 μm wavelengths.

Next, we investigate the effects of ice crystal size distributions and wavelengths (6.5 and 10.5 μm) on the cloud emissivity. Based on aircraft observations, Heymsfield (1975) presented two typical ice crystal size distributions for the cirrus uncinus (Ci) and Cs. The Ci distribution has a second peak at a crystal length of about 500 μm and consists of a great number of large crystals. In radiative transfer calculations, we also used

a third size distribution, which combines the other two by summing the Cs distribution and one-tenth of the Ci distribution and is denoted by Cs + Ci/10. This represents an intermediate ice crystal size distribution.

Using the preceding ice crystal size distributions and a number of cloud thicknesses (0.1 to 4 km), the cloud emissivity may be expressed in terms of the ice water path (IWP), i.e., the product of the ice water content (IWC) and cloud thickness, in units of g m^{-2}. Radiative transfer calculations were performed for the 6.5 and 10.5 μm wavelengths. Figure 1a shows the cloud emissivity as a function of the IWP for the three ice crystal size distributions. The wavelength dependence of the cloud emissivity appears to be quite small. However, the cloud emissivity depends significantly on the size distribution used. We reconstruct the data points, using the optical depth at the 0.55 μm wavelength as the scaling parameter. The optical depth is the product of the extinction coefficient and cloud thickness. Shown in Fig. 1b is the cloud emissivity plotted against the optical depth. The points $\triangle$, $\bigcirc$, and $\square$ are values taken from Fig. 1a. In the optical depth domain the dependence of the cloud emissivity on the cloud particle size distribution is not significant. There appears to be a unique relationship between the infrared cloud emissivity and visible optical depth. This optical relationship is independent of the ice crystal size distribution.

Using the cloud emissivity data computed from the radiative transfer program, we find that the emissivity
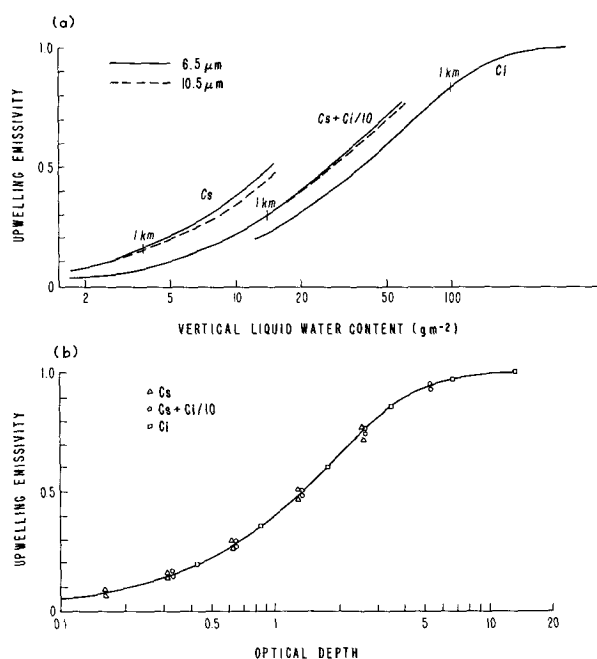

FIG. 1. (a) The upwelling emissivity as a function of the vertical liquid water content (or ice water path) for two wavelengths and three ice crystal size distributions identified in the graph. The number 1 km denotes the cloud thickness for each cloud type. (b) The upwelling emissivity as a function of the optical depth at 0.55 μm using the data from (a). The solid curve is the best fit to the data points.

may be parameterized in terms of the optical depth in the form

$$\epsilon = 1 - \exp(a\tau^b), \qquad (2)$$

where the coefficient a is -0.468 and b is 0.988. The correlation coefficient of the curve fitting is 0.98. In Eq. (2), when τ is 0, $\epsilon = 0$ and when $\tau \to \infty$, $\epsilon \to 1$. In this parameterization, the emissivity is expressed in terms of one parameter, namely, the optical depth at $0.55\ \mu m$. Since the dependence of the cloud emissivity on the ice crystal size distribution, cloud temperature, and wavelength has been removed through the optical depth scaling, this parameterized equation is useful for remote sounding applications involving cirrus clouds.

The ice crystal size distributions reported by Heymsfield (1975) and used in the present study have the lowest limit of maximum dimension at $20\ \mu m$. During STEP Australian flights, the measurements that were made on-board the ER-2 with a combined FSSP and 1-D probe (Knollenberg, personal communication) indicated the presence of a large number of small ice crystals with a diameter less than $20\ \mu m$. These measurements were carried out only near the cloud top and may not reflect the actual ice crystal size distribution throughout the entire cirrus layer. In recent years, there have also been suggestions that some of the cirrus clouds in midlatitudes may contain substantial numbers of ice crystals less than $20\ \mu m$ that have not been detected by optical probes. These suggestions were based on indirect radiometer, satellite, and lidar observations during the First ISCCP Regional Experiment (FIRE) carried out in Wisconsin, October–November 1987. While the direct evidence of small ice crystals less than $20\ \mu m$ in cirrus clouds has not been available at this point, their presence may have significant effects on the transfer of infrared radiation.

To investigate the potential effects of small ice crystals on the preceding cloud emissivity parameterization, three size distributions were used and extrapolated to $10\ \mu m$ on a logarithmic scale. Light scattering and radiative transfer calculations were subsequently performed. We have modified the program developed by Takano and Liou (1989a) based on the geometric ray-tracing technique. We estimate that this technique should be valid for particle size parameters X greater than about 20, where $X = 2\pi a/\lambda$, with a the radius and λ the wavelength. For X less than 20, we used the program developed by Asano and Sato (1980) for spheroids to calculate the single-scattering properties of small ice crystals. Naturally occurring ice crystals will have a hexagonal structure that cannot be accounted for by spheroids. However, according to Asano and Sato, the effects of shape on the scattering and absorption properties of small particles are generally small. This is an area that requires further investigation.

For Ci and Cs + Ci/10, the addition of small ice crystals has very little effect on the values of single-scattering albedo and phase function. This is in view

of the fact that these two size distributions consist of substantial numbers of large ice crystals. The cloud emissivity values with and without small ice crystals differ only in the second decimal point. Thus these differences can be neglected in the emissivity parameterization in terms of the opitcal depth. In the case of Cs, the number of large ice crystals decreases rapidly in the logarithmic scale. The inclusion of 10–20 μm sized ice crystals affects the single-scattering albedo, $\tilde{\omega}$, and asymmetry factor, g, slightly. For the 6.5 μm wavelength, we obtain $\tilde{\omega} = 0.551$ and $g = 0.919$ as compared with $\tilde{\omega} = 0.532$ and $g = 0.931$ without the addition of small ice crystals. For the 10.5 μm wavelength, we obtain ($\tilde{\omega} = 0.520$, $g = 0.946$) and ($\tilde{\omega} = 0.530$, $g = 0.949$) for cases with and without small ice crystals, respectively. In both cases, the asymmetry factor does not have sufficient variations to cause changes in the emissivity results. The single-scattering albedo for the 6.5 μm wavelength increases with the addition of 10–20 μm sized ice crystals because there is more scattering in the case with small ice crystals. However, for the 10.5 μm, the behavior of the single-scattering albedo is reversed. This is explained by the increase of absorption efficiency for very small size parameters. With the addition of small ice crystals, the cloud emissivity values decrease and increase within about 0.02 and 0.04 for 10.5 and 6.5 μm, respectively. However, these changes do not have a significant effect on the parameterization of the cloud emissivity as a function of the visible optical depth. Using Eq. (2), we find that the best fit to the data points, including cases with small ice crystals, has the coefficients $a = -0.469$ and $b = 0.991$. The computed optical depth from the known cloud emissivity is affected only on the second decimal point.

Having discussed the parameterization of the cloud emissivity in terms of the optical depth and the potential effects of small ice crystals on the parameterization, we shall formulate the retrieval program for the determination of the cloud emissivity and cloud temperature. Based on lidar observations presented by Platt et al. (1987), tropical cirrus clouds have an averaged base height of 13 km. To a first approximation, the reflection effect at thermal infrared wavelengths may be neglected when the cloud is viewed from above. The upwelling radiance at the cloud top for a given channel i, I_i, can be expressed by the sum of transmission of the radiance reaching the cloud base, I_{bi}, and emission from the cloud. Let the effective cloud temperature be T_c, then the upwelling radiance at the cloud top may be written as

$$I_i = I_{bi}(1 - \epsilon) + \epsilon B_i(T_c) \begin{cases} i = 1, & 6.5\ \mu m \\ i = 2, & 10.5\ \mu m. \end{cases} \qquad (3)$$

In order to infer the cirrus emissivity, ϵ, and temperature, T_c, from two radiance measurements in cloudy conditions, the upwelling radiances at the cloud base,

I_{bi}, must be known. In addition, the nonlinear Planck functions B_1 and B_2 must be related. In principle, I_{bi} may be obtained from forward radiation transfer calculations if the surface temperature, temperature and humidity profiles, and cloud base height are given. This approach requires information about several parameters and appears to be impractical. A more direct and reliable method to determine I_{bi} would be to find clear column radiances from the data available. In the case of tropical anvils that are located at a height of 13 km or higher, the upwelling radiances for the two wavelength channels at the level of the cloud base are about the same as those at the ER-2 flight level that is typically 19–20 km for clear sky conditions. This is because there is little water vapor present above about 10 km. The upwelling radiances above 10 km vary only insignificantly (<0.1% of the value at 15 km). Based on numerical analyses, we find that B_1 and B_2 may be related via the following equations:

$$B_1(T) = f[B_2(T)]$$

$$= \begin{cases} \sum_{n=1}^{4} a_n B_2^{n-1}(T), & T \geq 210 \text{ K} \\ b[B_2(T)]^c, & T < 210 \text{ K} \end{cases} \quad (4)$$

where $a_1 = -0.37209$, $a_2 = 0.0847$, $a_3 = 2.4106 \times 10^{-3}$, $a_4 = -4.789 \times 10^{-6}$, $b = 0.02039$, and $c = 1.5672$. The accuracy of the fitting of the Planck function is better than about 1%.

Using the Planck function relationship denoted in Eq. (4), Eq. (3) may be rewritten in the form

$$\left.\begin{array}{l} I_1 = I_{b1}(1 - \epsilon) + f(B_2)\epsilon \\ I_2 = I_{b2}(1 - \epsilon) + B_2\epsilon \end{array}\right\}. \quad (5)$$

On eliminating ϵ, we obtain

$$f(B_2) = SB_2 + R, \quad (6)$$

where

$$\left.\begin{array}{l} S = (I_1 - I_{b1})/(I_2 - I_{b2}) \\ R = I_{b1} - SI_{b2} \end{array}\right\}. \quad (7)$$

Equation (6) is a linear equation relating $f(B_2)$ and B_2, where S is the slope and R the intercept. Since the clear-column radiance values (I_{b1}, I_{b2}) also satisfy Eq. (6), the slope can be determined by Eq. (7). We use Eqs. (4) and (6) to determine B_1 [or $f(B_2)$] and B_2 on the basis of a numerical iterative scheme similar to Newton's iteration method, which is noted for its accuracy and efficiency. In this scheme, we find the intersection of the two curves represented by Eqs. (4) and (6) to obtain B_1. From the Planck function, the cloud temperature can be computed. Subsequently, the cloud emissivity can be determined from Eq. (5). A description of the numerical program for the retrieval of Planck functions is given in the Appendix.

3. Application to STEP data

The STEP experiments over Australia were carried out during January–February 1987 with a total of 14 flight missions. From an inspection of the flight tracks along with GMS satellite cloud pictures, we find that the data collected during flights 9 and 12 are most appropriate for the present retrieval analysis. This is in view of the fact that the measured radiance data for these two flights were well-calibrated and that the flight tracks were confined to relatively small areas to warrant uniform clear sky temperatures below the cloud. Also there were reasonably well-defined clear and cirrus overcast regions. The radiances for the 6.5 and 10.5 μm channels were measured from the dual-channel nadir-viewing radiometers, which have a field-of-view of about 8° and a response time of about 50 ms^{-1}. The radiometers were continuously chopped for calibration against a liquid nitrogen blackbody to ensure accuracy and stability. For every second, 18 measurements were made by the radiometer, but only two measurements per second were selected because of the limitation of the computer storage of data points. The radiometers measured the energy in units of W m^{-2} per 1 μm band width per steradian. In the processing of the measured data, a calibration procedure was made so that the band filter over the 1 μm band width is a square function. Thus the radiance values from measurements correspond to the center wavelengths; i.e., 6.5 and 10.5 μm.

a. Flight 9

STEP flight 9 was flown on 1 February 1987. On that date, a cyclone was developing west of the Kimberlies. This cyclone generated several active cloud bands in moderately strong maritime westerlies to the north of Darwin. The ER-2 took off at 0700 (local time) from Darwin and flew a series of five vertically stacked legs oriented south-southwest to north-northeast over the Timor Sea from the north coast of Australia to the south coast of Indonesia. Each leg was approximately 500 km long. Successive legs were flown at altitudes of 15.24, 15.85, 16.46, 17.07, and 18.29 km. The objective of the mission was to carry out measurements within and above an extended cirrus outflow region. This outflow, as seen on the GMS 10 μm cloud picture depicted in Fig. 2, was several hundred kilometers across (north to south) and about 1000 km long (east to west). The dots in this picture indicate the approximate flight track.

On inspecting the radiance time series, we find that there are distinct maxima and minima for the first half of the flight. The data for the latter half of the flight are relatively featureless. For retrieval analyses, we selected the data from $t = 82\,000$ sec to $t = 92\,000$ sec (UTC) on 31 January 1987, corresponding to the first half of the flight. Every 2000 sec of the flight corresponds approximately to 400 km, based on an average
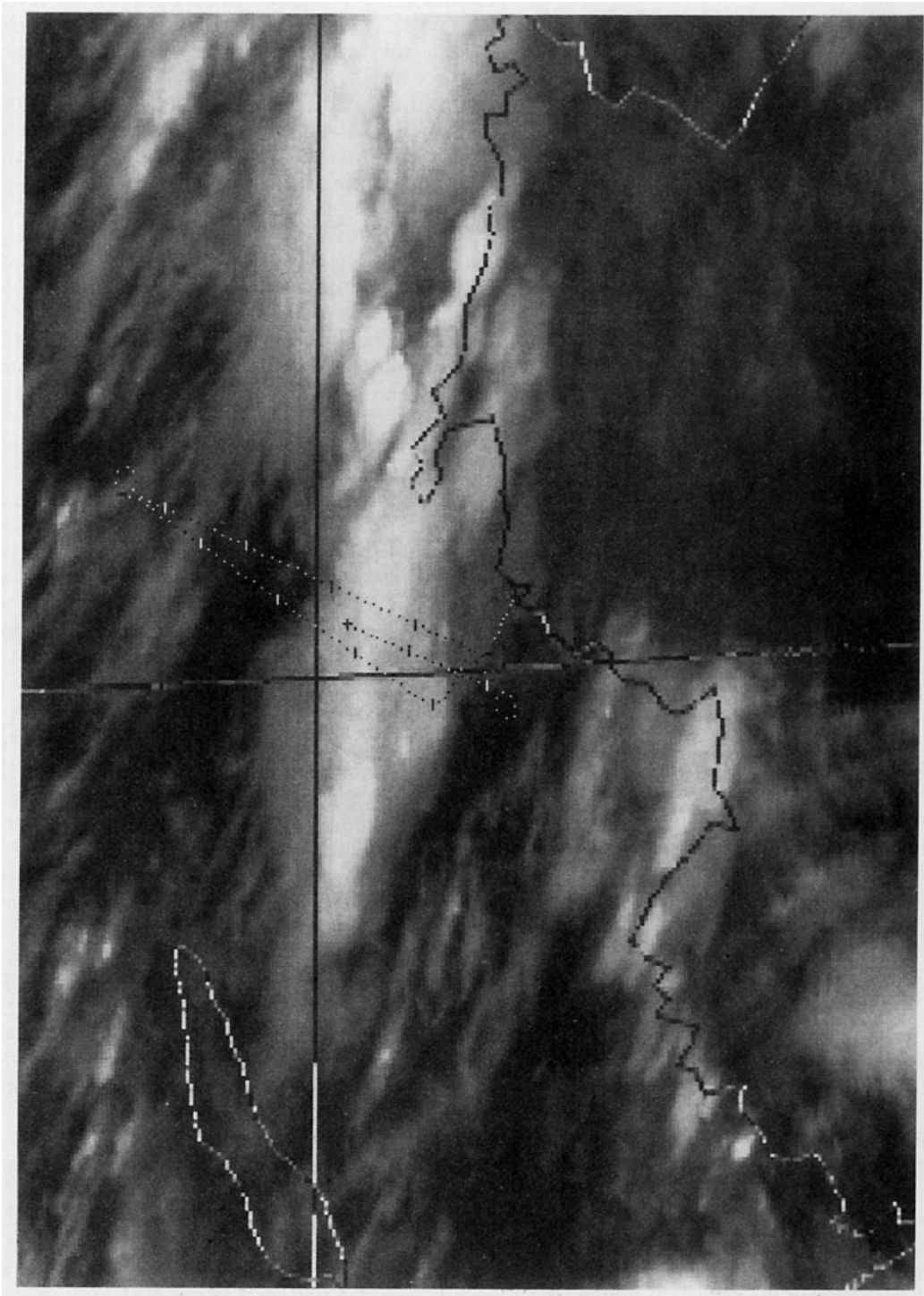
FIG. 2. GMS infrared picture at 21Z, 31 January 1989. The dots in this picture approximately indicate the STEP flight 9 track. The vertical and horizontal lines in the picture correspond to 10°S and 130°E, respectively.

aircraft speed of 200 m s^{-1}. The total time interval of the flight was about three hours. Using an average wind speed of 20 m s^{-1}, clouds would move a distance of about 200 km. Although the cloud field changes during the flight, the clear-sky temperatures are relatively uniform horizontally, as evidenced by the temperature profile measured during the ascent and descent of the aircraft. Thus the brightness temperature pair (T_{b1}, T_{b2}) measured in a few clear regions can be applied to the entire area covered by the flight for retrieval purposes.

The flight track was divided into 10-min intervals. The data that was selected for analysis begins at the fifth interval and ends at the twenty-first interval. The first four intervals correspond to the ascent period of the aircraft. Figures 3a and 3b show the radiance time series for channels 1 (6.5 μm) and 2 (10.5 μm), respectively. Large values correspond to relatively clear conditions, whereas small values are associated with

emission from overcast regions. From the time series, it is evident that the minima around 8.5×10^4, 8.7×10^4, and 9×10^4 sec were obtained over overcast regions, while maximum values around 8.6×10^4, 8.9×10^4, and 9.1×10^4 sec were obtained over clear areas. The brightness temperatures corresponding to the maximum and minimum radiances converted from the Planck function are about 240 and 190 K, respectively, for the 6.5 μm channel. For the 10.5 μm channel, they are 280 and 190 K, respectively. Since the minimum values for both channels are about the same, radiation must come primarily from cloud emission. The value of 190 K corresponds to the cirrus cloud top temperature, revealing that the overcast cirrus is radiatively black. This is supported by the ER-2 ambient temperature measurements made on the lower flight legs. The maximum brightness temperatures for both channels are close to the ambient temperature at the level of the weighting function peak, which is about 9 km for the 6.5 μm channel and about 2 km for the 10.5 μm channel.

To retrieve the cloud temperature and emissivity, the upwelling radiances reaching the cloud base must be known. As noted previously these radiances are approximately the same as those measured in clear conditions in the case of tropical cirrus. Thus our first task is to seek representative clear column radiances from the datasets. For this purpose, a statistical analysis was first performed. The radiance ranges for the 6.5 μm (I_1) and 10.5 μm (I_2) channels are 0–1.5 and 0–12 W/ (m^2·sr), respectively. We then divide I_1 and I_2 into 30 and 24 values, with discrete intervals of 0.05 and 0.5 W/(m^2·sr), respectively. Thus there are a total of 720 interval pairs. Subsequently, the observed radiance data are assigned to these intervals to obtain the frequency of occurrence. Figure 4 shows the three-dimensional frequency distribution based on the datasets
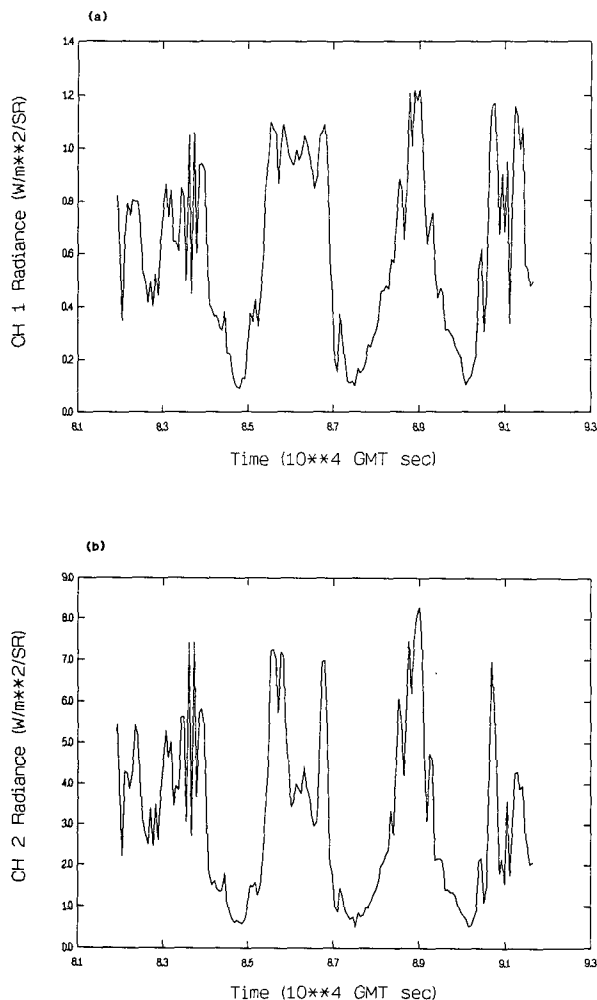

FIG. 3. (a) Time series of the radiance for 6.5 μm (Channel 1) derived from the ER-2 nadir-viewing radiometer for the STEP flight 9. (b) Same as (a), except for 10.5 μm (Channel 2).
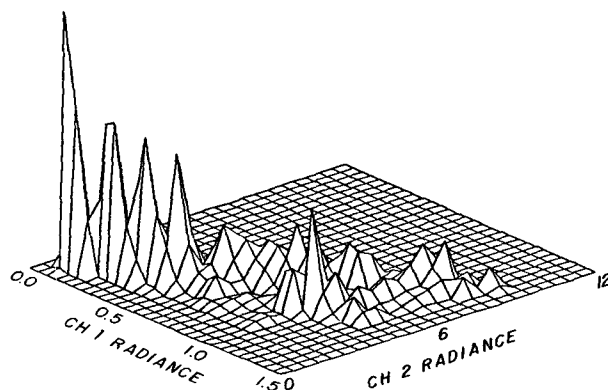

FIG. 4. Frequency of occurrence of the radiance pair, 6.5 (Channel 1) and 10.5 (Channel 2) μm. The largest radiance values are associated with clear conditions. High frequency of occurrence of small radiances indicate that tropical cirrus clouds under the present study tend to be optically thick.

that are used in the analysis. The pair (I_1, I_2) with the lowest values of 0.13 and 1 W/$(m^2 \cdot sr)$ has the highest frequency of occurrence. It is clear that a major portion of the data collected during the experiment is associated with optically thick cirrus. That tropical cirrus can be optically thick, with emissivities close to 1, has been observed by Griffith et al. (1980) and inferred from satellite imagery (Ackerman et al. 1988). In the lower right corner of Fig. 4, the last significant peak occurs near the pair (I_1, I_2) with values of 1.3 and 8.75 W/$(m^2 \cdot sr)$. These are the largest radiances and are presumably associated with clear sky conditions.

Using the retrieval scheme described in section 2, the time series of the computed cloud temperature and emissivity is shown in Figs. 5a and 5b, respectively. In addition, the computed optical depths are displayed in Fig. 5c. The present retrieval program for the cloud temperature and emissivity is based on the presumption that high cirrus clouds are present. Thus there would be no information for the cloud temperature in the cases of clear conditions; i.e., $\epsilon = 0$, as evident from Eq. (5). In practice, when the observed radiance I_1 (or I_2) differs from the clear sky radiance I_{b1} (or I_{b2}) by less than 10%, the pair (I_1, I_2) is rejected in the retrieval. This is in consideration of the uncertainty in the determination of the slope, S, denoted in Eq. (7). The minimum and maximum retrieved cloud temperatures are about 190 and 230 K, respectively. As pointed out previously, the 190 K value corresponds to the cloud top temperature of optically thick cirrus. Also, the 230 K value is close to the maximum brightness temperature of the 6.5 μm channel. Some of the larger emissivity values retrieved appear to correspond to lower cloud temperatures, as shown in Figs. 5a and 5b. However, there is no definitive functional dependence between the two variables. The emissivity approaches unity for optically thick cirrus clouds with lower temperatures. Other emissivity values vary between 0 and 0.8, corresponding to clear columns, thin cirrus, and the boundaries of thick cirrus. The optical depth is computed from Eq. (2) based on the emissivity parameterization. The computed emissivity and optical depth vary significantly along the flight path. For thin cirrus and partly covered thick cirrus within the field-of-view of the radiometers, the optical depths vary between about 0.5 and 5. For thick cirrus clouds, the optical depths are greater than 6.

b. Flight 12

STEP flight 12 was flown on 8 February 1987, during which a cyclone (Jason) was present over the northern Gulf of Carpentaria. Cirrus cloud bands extended northward and westward from the center of the cyclone. The ER-2 took off at 1000 (local time) from Darwin and flew east, crossing the northern part of Australia, circling over the cyclone, and then flying back to Darwin. It took about 40 min to reach the edge of the
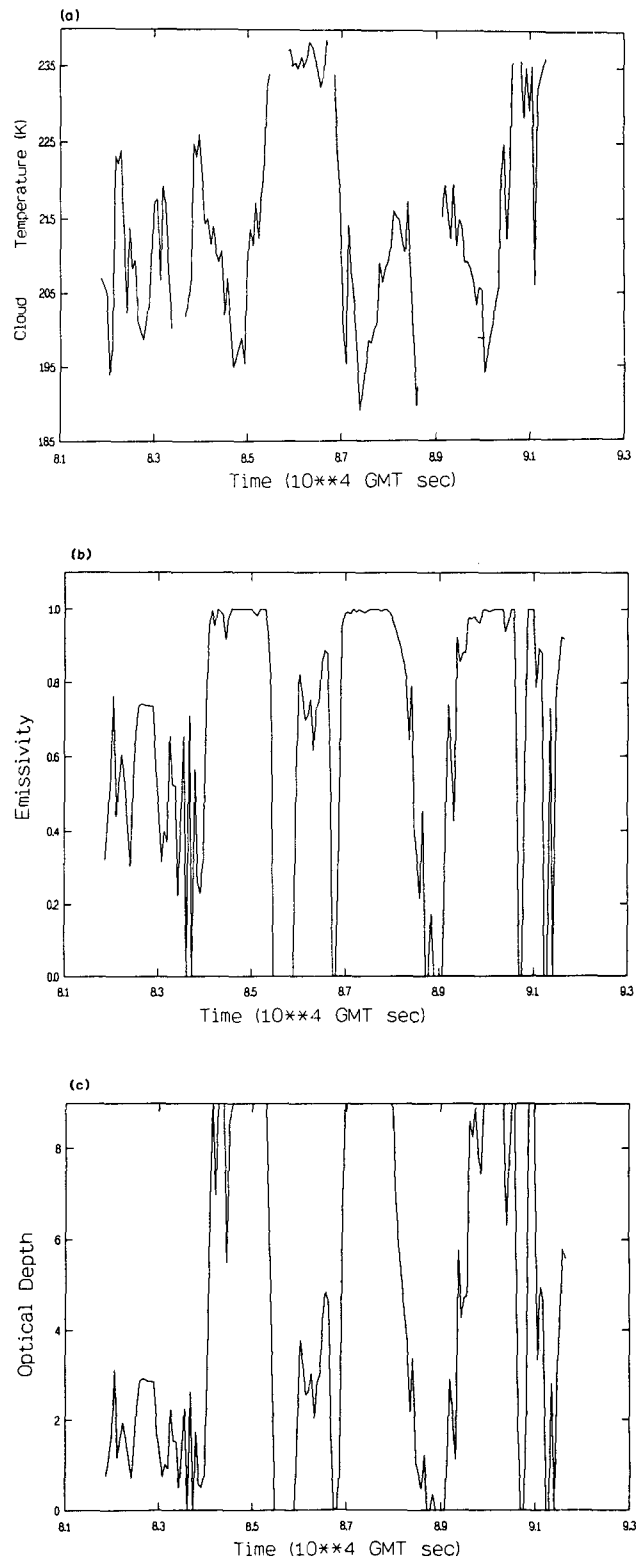

FIG. 5. (a) The retrieved cloud temperature as a function of time for the STEP flight 9. (b) Same as (a), except for the cloud emissivity. (c) Same as (a), except for the optical depth. Note that the largest optical depth that can be determined reliably from the present retrieval algorithm is about 6.

cirrus cloud band. The flight maintained an altitude range between 18 and 20 km.

There are distinct maxima and minima radiances for the entire flight. The radiance data from $t = 6110$ sec to $t = 20\ 136$ sec (UTC) on 8 February 1987 were selected for the retrieval analysis. The total time interval of the flight was about five hours. Figures 6a and 6b show the radiance time series for channels 1 and 2. Minimum radiances are seen at about 0.8×10^4, 1.0×10^4, 1.3×10^4, and 1.6×10^4 sec, while maximum radiances are seen at about 0.9×10^4, 1.2×10^4, 1.8-1.9×10^4 sec. The brightness temperatures that correspond to the maximum and minimum radiances are about 240 and 210 K, respectively, for the 6.5 μm
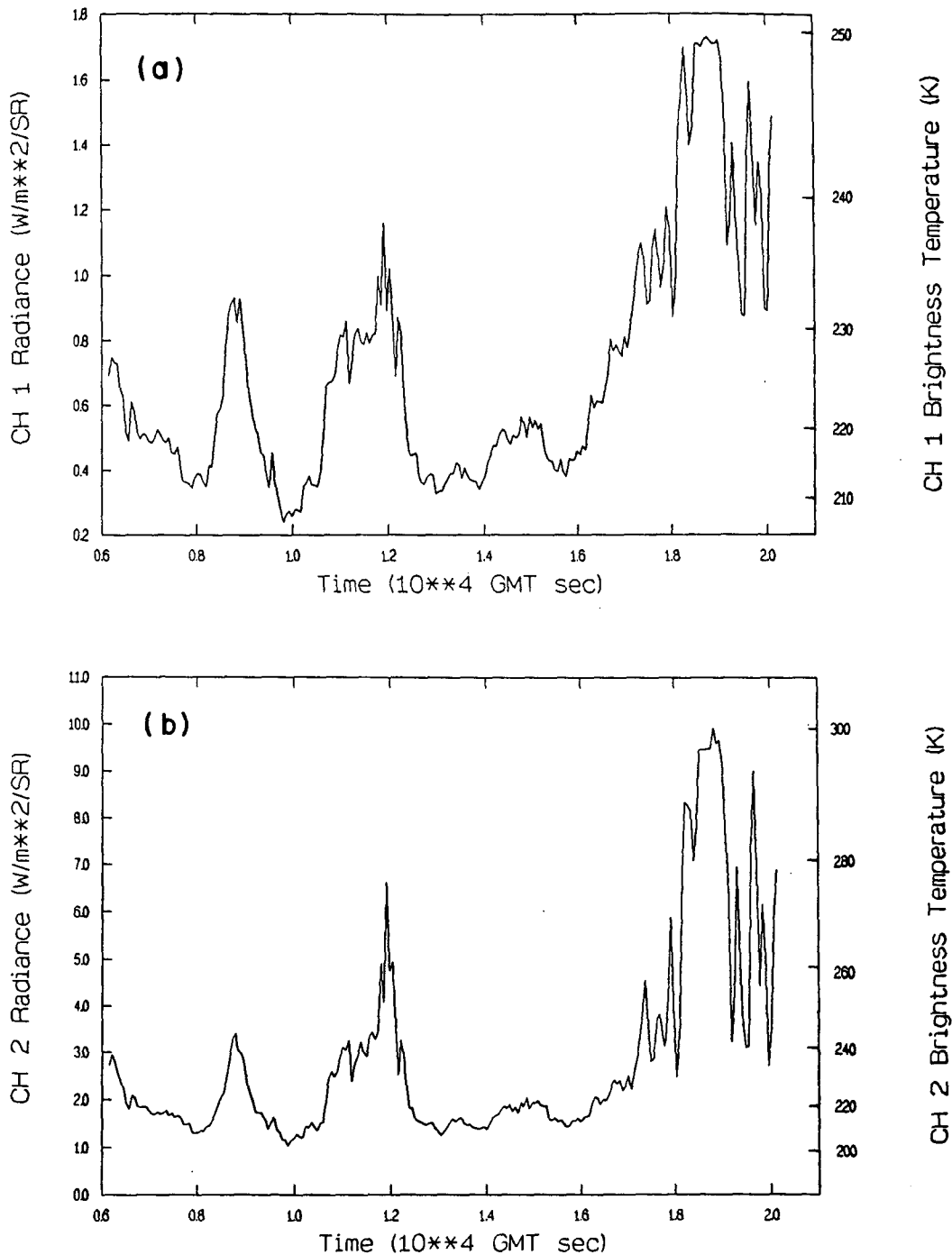

FIG. 6. Same as (3), except for STEP flight 12.

channel. For the 10.5 μm channel, the minimum brightness temperature is also about 210 K, but the maximum brightness temperature ranges between 230 and 280 K. The minimum brightness temperature of 210 K is higher than that of 190 K computed from the flight 9 data, indicating a lower cloud top height. Radiances over the thick cirrus area must come primarily from cloud emission. The maximum values for the 6.5 μm channel are close to the temperature at the level of the weighting function peak at about 9 km. However, variations in the maximum radiances for the 10.5 μm channel indicate the possible presence of low level clouds.

Using the retrieval technique described in section 2, which includes the search of clear column radiances based on a three-dimensional frequency distribution method, the time series of the computed cloud temperature and emissivity are shown in Figs. 7a and 7b, respectively. The optical depths computed from the emissivity parameterization are displayed in Fig. 7c. The minimum and maximum retrieved cloud temperatures are about 200 and 240 K, respectively. As noted earlier, the 200 K value corresponds to the cloud top temperature of optically thick cirrus clouds. The value of 240 K is close to the maximum brightness temperature of the 6.5 μm channel. The retrieved cloud emissivity values vary between about 0.2 and 1.0. These values are similar to those retrieved from the flight 9 data. The time series of the optical depth follows the pattern of the cloud emissivity. Over the area of thin and moderately thick cirrus clouds, optical depths vary between about 0.5 and 6.

c. Some verification of the retrieved results

There were no concurrent cloud temperature profiles and cloud physics measurements made during the experiment from which the retrieved temperature and optical depth can be verified directly. If the ice crystal size distribution were provided from measurements, then the extinction coefficient could have been computed from a light scattering program for hexagonal particles. Mutiplication of the extinction coefficient with the measured cloud thickness would give the cloud optical depth. Although a direct validation of the retrieved result is not possible, we find that the data presented by Platt et al. (1987) and Griffith et al. (1980) may be used to cross-check the present results. The former authors carried out lidar and infrared radiometer experiments to derive the cirrus cloud properties at Darwin, Australia in March 1981. They concluded that the midcloud temperatures of tropical cirrus are mostly between 193 and 233 K. The present values are in general agreement with their results. According to our previous discussion, we must have the extinction coefficient for ice crystals and cloud thickness to verify the optical depth. Platt et al. (1987) reported that the thickness of tropical cirrus ranges from
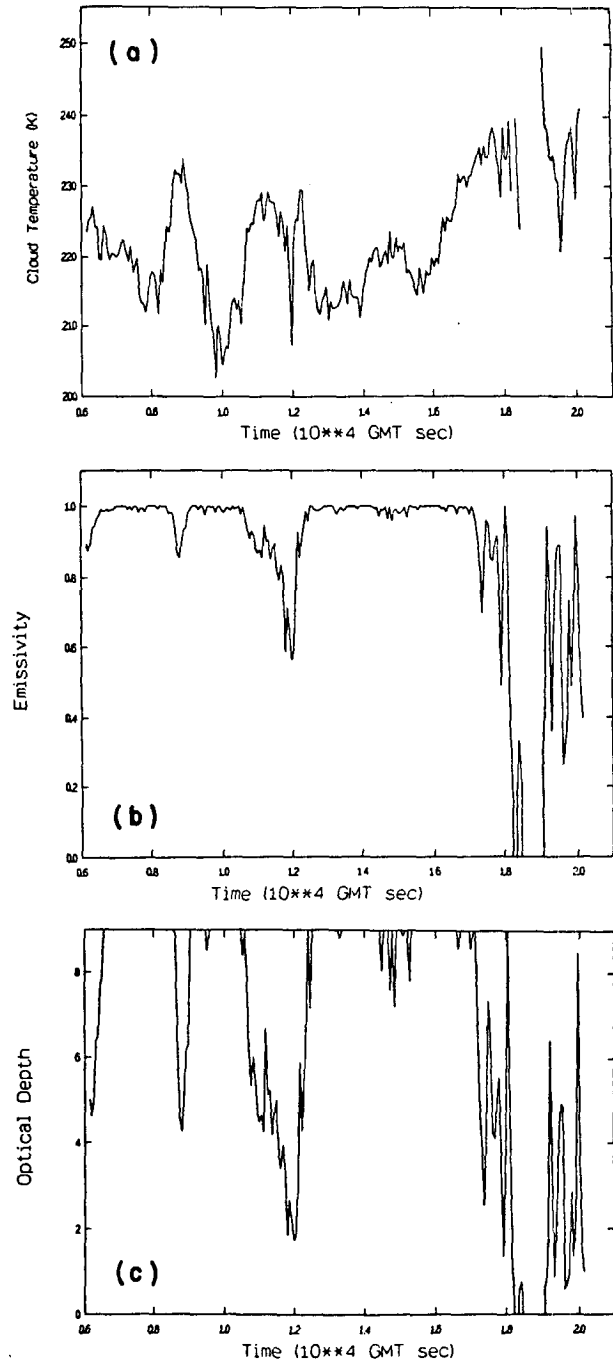

FIG. 7. Same as (5), except for the STEP flight 12.

about 1 to 3 km. Moreover, Griffith et al. (1980) obtained the ice crystal size distribution from a one-dimensional optical array particle spectrometer for thick tropical cirrus and derived values of 0.03–0.08 g m^{-3} for the ice water content. It should be noted that their measurements were made over the Atlantic GATE region and at substantially lower altitudes. Also, they did not have the capability to measure small ice crystals.

As pointed out in section 2, the cloud physics measurements that were made on-board the ER-2 indicated the presence of a large number of small ice crystals, with diameter $d < 20$ μm. Unfortunately, all the STEP cloud physics measurements were made near the cloud top and did not represent the actual ice crystal size distribution throughout the entire cirrus layer. In order to estimate the optical depth, we shall use the results reported by Griffith et al. and assume that the shapes of ice crystals are hexagonal columns. The mass extinction cross section was found to be in the range of 0.076–0.096 m^2 g^{-1}. It follows that the extinction coefficient for ice crystals would be on the order of 2.28 to 7.68 km^{-1}. Combining these extinction coefficients with the cloud thicknesses reported by Platt et al., the optical depth for thick tropical cirrus is on the order of about 2 to 20. In the present study, the optical depth is computed from the retrieved cloud emissivity through a parameterized equation, which is in the form of an exponential function. Because of the behavior of the exponential function, the upper limit of the optical depth that can be computed is about 10. From the satellite imagery, we note that thin cirrus clouds were present during STEP flight 9. Thus the optical depths computed from the current study that vary from about 0.5 to >10 appear to be reasonable.

4. Conclusions

A dual-channel technique using 6.5 and 10.5 μm wavelengths for the retrieval of the temperature and emissivity of tropical anvils has been developed. This technique is based on a theoretical parameterization of the cloud emissivity as a function of the optical depth at 0.55 μm. In the optical depth domain, the effective cirrus emissivity is largely independent of the ice crystal size distribution and wavelength at 6.5 and 10.5 μm. In the development of the retrieval algorithm, concurrent clear-column radiances are required in order to reduce the unknown variables to two, namely, the cloud temperature and cloud emissivity.

Applications of the retrieval program to the STEP data have been carried out. These data were obtained by the ER-2 6.5 and 10.5 μm downward looking radiometers over the vicinity of Darwin, Australia, 1 February 1987. From the available datasets, a statistical analysis has been performed to obtain the radiance pair that corresponds to the clear column. We show that the retrieved cloud temperatures are between 190 and 240 K, in general agreement with the results derived from the lidar observations (Platt et al. 1987). The retrieved cirrus emissivities range between 0.2 and 1. A large portion of the tropical cirrus clouds sampled during STEP flights 9 and 12 appear to be optically thick, with their emissivities close to 1. The optical depths are determined from the cloud emissivity via a parameterization. Due to the exponential behavior of

the parameterized equation, the largest optical depth that can be derived reliably from the present study is about 6. While the retrieved cloud emissivity and optical depth values for tropical cirrus clouds appear to be qualitatively correct, a quantitative verification of these results is not possible without concurrent and detailed cloud physics measurements. Finally, it should be noted that in order to determine more precisely the optical depths for thick cirrus clouds, additional channel(s) in the solar spectral region must be used.

APPENDIX

Numerical Solution for B_2 and $f(B_2)$

Based on Eq. (4), an initial guess of B_2, say $B_2^{(0)}$, is made: $f[B_2^{(0)}]$ can then be computed. Subsequently, the derivative of the Planck function curve at the point $B_2^{(0)}$ is given by

$$f'[B_2^{(0)}] = \sum_{n=1}^{3} n a_{n+1} [B_2^{(0)}]^{n-1}. \quad (A1)$$

Here, we have used the cases when $T^{(0)} > 210$ K. The linear equation for the tangent curve at the point $B_2^{(0)}$ may be written in the form

$$f^*(B_2) = f'[B_2^{(0)}][B_2 - B_2^{(0)}] + f[B_2^{(0)}], \quad (A2)$$

where the function f^* differs from f defined in Eq. (4). The tangent curve intersects the line represented by Eq. (6). This intersection may be denoted by $B_2^{(1)}$ and $f^*[B_2^{(1)}]$ where

$$B_2^{(1)} = \{f[B_2^{(0)}] - R$$
$$- f'[B_2^{(0)}]\}/\{S - f'[B_2^{(0)}]\}, \quad (A3)$$

and

$$f^*[B_2^{(1)}] = SB_2^{(1)} + R. \quad (A4)$$

These procedures are repeated to obtain $B_2^{(n)}$ and $f^*[B_2^{(n)}]$, where $n = 2, 3, \cdots$, until a converged solution is reached; i.e.,

$$[B_2^{(n)} - B_2^{(n-1)}]/B_2^{(n)} \leq \delta, \quad (A5)$$

where δ is a prescribed convergence criterion. In the present method, we find the intersection between the Planck function curve and a straight line. It is similar to Newton's iterative method, which has been widely used to find the intersection between a curve and the abscissa. Both methods use tangential lines to accelerate the convergence.

JOURNAL OF APPLIED METEOROLOGY

REFERENCES

Ackerman, T. P., K. N. Liou, F. P. J. Valero and L. Pfister, 1988: Heating rates in tropical anvils. *J. Atmos. Sci.,* **45,** 1606–1623.

Asano, S., and M. Sato, 1980: Light scattering by randomly oriented spheriodal particles. *Appl. Opt.,* **19,** 962–974.

Griffith, K. T., S. K. Cox and R. G. Knollenberg, 1980: Infrared radiative properties of tropical cirrus clouds inferred from aircraft measurements. *J. Atmos. Sci.,* **37,** 1077–1087.

Heymsfield, A. J., 1975: Cirrus uncinus generating cells and the evolution of cirroform clouds. Part I: Aircraft observations of the growth of the ice phase, *J. Atmos. Sci.,* **32,** 799–808.

Huang, R., and K. N. Liou, 1984: Remote sounding of cirrus optical depth and temperature from 3.7 and 11 micrometer windows. *Adv. Atmos. Sci.,* **1,** 150–164.

Liou, K. N., 1977: Remote sensing of the thickness and composition of cirrus clouds from satellites. *J. Appl. Meteor.,* **16,** 91–99.

——, 1986: Influence of cirrus clouds on weather and climate processes: A global perspective. *Mon. Wea. Rev.,* **114,** 1167–1199.

Pollinger, W., and P. Wendling, 1984: A bispectral method for the height determination of optically thin ice clouds. *Contrib. Atmos. Phys.,* **57,** 269–281.

Platt, C. M. R., J. C. Scott and A. C. Dilley, 1987: Remote sensing of high clouds. Part VI: Optical properties of midlatitude and tropical cirrus, *J. Atmos. Sci.,* **44,** 729–747.

Szejwach, G., 1982: Determination of semi-transparent cirrus cloud temperature from infrared radiances: Application to METEO-SAT. *J. Appl. Meteor.,* **21,** 384–393.

Takano, Y., and K. N. Liou, 1989a: Solar radiative transfer in cirrus clouds. Part I: Single-scattering and optical properties of hexagonal ice crystals, *J. Atmos. Sci.,* **46,** 3–19.

——, and ——, 1989b: Solar radiative transfer in cirrus clouds. Part II: Theory and computation of multiple scattering in an anisotropic medium, *J. Atmos. Sci.,* **46,** 20–36.